

Local inhibitory networks support up to $(N - 1)!/\ln^N 2$ limit cycles in the presence of electronic noise and heterogeneity

Ashok S. Chauhan¹, Joseph D. Taylor, and Alain Nogaret^{1*}

Department of Physics, University of Bath, Bath BA2 7AY, United Kingdom



(Received 24 August 2021; accepted 21 October 2021; published 3 November 2021)

A paradox in neuroscience is the large number of oscillations of small neural networks compared with the few oscillations observed in the conscious brain. It remains unclear what is the maximum number of synchronized oscillations a network can support and whether all or some of these oscillations would survive in noisy heterogeneous circuits. Here, we attempt to answer these questions through a comprehensive study of local inhibitory networks of Hodgkin-Huxley neurons. We use a neuromorphic platform combining electronic noise and device-specific heterogeneity with tuneable extrinsic noise, tuneable network connectivity, and controlled initial conditions. As in the brain, stimuli are instantaneously integrated by analog circuits. This gives us the computing power needed to map the network dynamics over the entire phase space and demonstrate the full complement of limit cycles, basins of attraction, and dependence on network parameters. Our main finding is that the maximum number of limit cycles is equal to the combinatorial number of activation pathways through the network, allowing for coincident action potentials, and that all limit cycles are equally robust to noise and mild heterogeneity but highly dependent on inhibition delay and the timing of stimuli. We established the robustness of individual limit cycles by computing the detailed balance of bifurcations between attractors. This accounts for all transitions in a system where Lyapunov exponents are both positive and negative depending on phase space coordinates and noise intensity. Another interesting finding is the unexpected resilience of limit cycles to mild network heterogeneity. This occurs as stochastic processes recruit quiescent neurons whose subthreshold periodic oscillations help maintain the synchronization of limit cycles against heterogeneity.

DOI: [10.1103/PhysRevResearch.3.043097](https://doi.org/10.1103/PhysRevResearch.3.043097)

I. INTRODUCTION

Neuronal synchronization in the brain occurs over a few frequency bands corresponding to the δ , θ , α , β , and γ brain waves [1]. The search for mechanisms explaining this synchronization [2–8] and the formation of spatial patterns such as spindle, radial, and standing waves [9,10] has attracted considerable interest. In contrast, local networks support different modes of synchronized oscillations activated with appropriate stimulation. Switching between oscillatory modes is known to be elicited by stimuli in central pattern generators underpinning escape swimming in *Tritonia* [11] and the sea slug [12]. Recently, specialized interneurons have been identified that can elicit different responses from central pattern generators in tadpoles and zebrafish [13]. Theoretical simulations of a three-neuron inhibitory network predict up to six stable patterns of spatiotemporal oscillations [14–16]. More generally, a network of N inhibitory neurons with all-to-all connectivity is expected to host a huge complement of $(N - 1)!/\ln^N 2$ stable oscillatory states [17]. The dynamic limit cycles as-

sociated with these states are expected to be robust to noise since moderate noise levels give negative Lyapunov exponents [18–20]. One may therefore question why so few oscillations are observed in the brain compared with the huge number of theoretically possible states; what is the maximum number of oscillations an experimental network can host; and whether some or all of these oscillations would survive in the noise and heterogeneity of the brain.

Here, we investigate the oscillation patterns of two-, three-, and four-neuron inhibitory networks in a neuromorphic device with which we demonstrate the maximum number of $(N - 1)!/\ln^N 2$ limit cycles in a noisy and heterogeneous environment. We elicited all possible oscillatory states of the network by varying the timing of electrical stimuli. We find that the maximum number of oscillations is strongly dependent on the delay of the inhibitory postsynaptic potential (IPSC) relative to the presynaptic action potential (AP). This delay allows coincident APs and hence coherent and partially coherent modes of oscillation. A small delay, $d = 300 \mu\text{s}$ (30% of the AP width), is sufficient to stabilize the maximum number of oscillations a network can support. Our experiments also recognize that phasic oscillations may alternatively be induced by making the IPSC recovery time τ commensurate with the oscillation period T in the ratio $T/\tau \approx 14$. This validates earlier observations [2,21,22]. However, we find that the commensurability criterion is generally weaker than the inhibition delay criterion, especially in larger networks ($N > 2$) where the former requires a minimum inhibition delay.

*A.R.Nogaret@bath.ac.uk

Published by the American Physical Society under the terms of the [Creative Commons Attribution 4.0 International](https://creativecommons.org/licenses/by/4.0/) license. Further distribution of this work must maintain attribution to the author(s) and the published article's title, journal citation, and DOI.

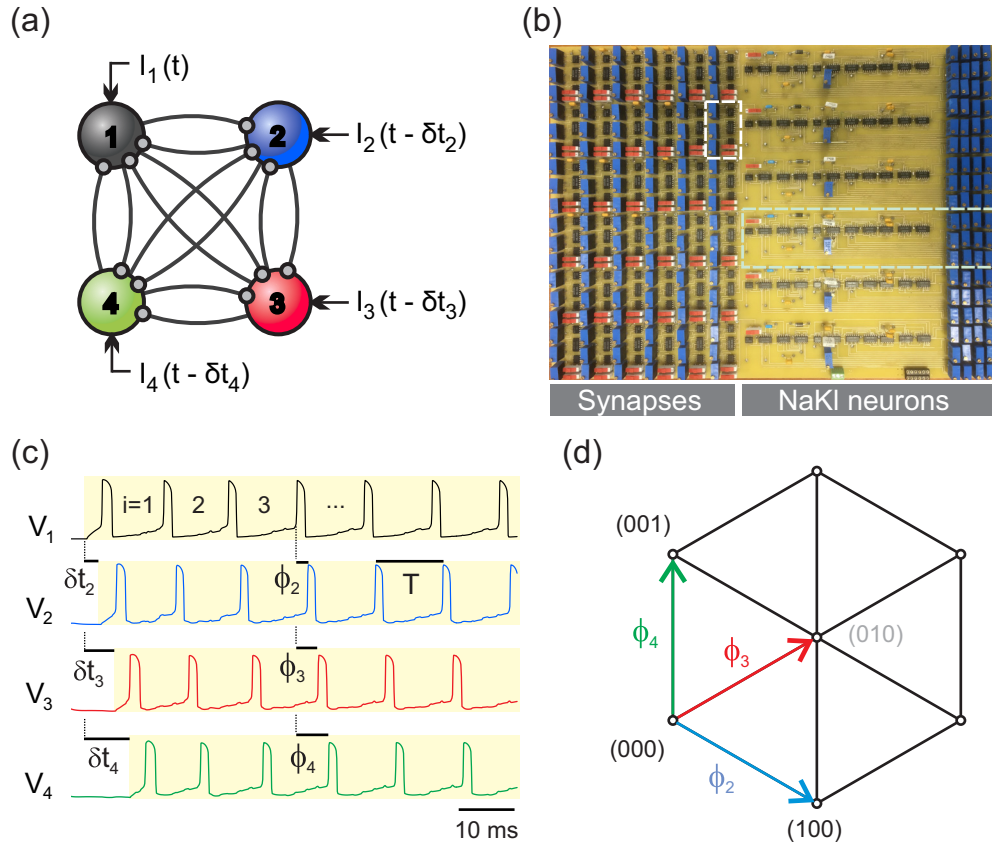


FIG. 1. Neuromorphic inhibitory network. (a) Network of four neurons interconnected with inhibitory synapses. The four neurons were stimulated with current steps of equal amplitude. The steps applied to neurons 2, 3, and 4 were delayed by δt_2 , δt_3 , and δt_4 relative to neuron 1. (b) Analog inhibitory network comprising six NaKl neurons interconnected with a matrix of 6×6 synapses. A single neuron (synapse) is shown in the green (white) dashed box. (c) Example of spatiotemporal oscillations (solid lines) elicited by delayed current steps (yellow shading). Oscillations are recorded over the first 50 periods, during which the transient regime evolves into a synchronized state. The state of the network is represented by the dephasings ϕ_2 , ϕ_3 , and ϕ_4 of neurons 2, 3, and 4 relative to neuron 1. (d) Orthographic projection of the three-dimensional space mapping the time evolution of the state vector (ϕ_2 , ϕ_3 , ϕ_4).

Network-specific heterogeneity came from tolerances on electronic components. We systematically varied synaptic conductances to study the network dynamics during the gradual transition from all-to-all connectivity to a clockwise projecting neuron ring. We unexpectedly find that the limit cycles of the all-to-all network remain intact even after 8 out of 12 synaptic conductances have been halved. We explain this unexpected stability by the entrainment of subthreshold neurons whose periodic oscillations may be transmitted stochastically. This mechanism is neglected in numerical simulations [14,15]; however, it efficiently stabilizes the oscillatory states of physical networks against heterogeneity. Intrinsic noise came from $1/f$ electronic and thermal noise. In addition, we applied extrinsic noise by adding Gaussian noise to current stimuli. This allowed us to study the detailed balance of transitions between limit cycles and observe the robustness of limit cycles to noise. These results demonstrate the one-to-one correspondence of limit cycles to cyclically ordered activation pathways. They validate the combinatorial derivation of the maximum number of oscillatory states [17]. We discuss possible reasons for which the large number of predicted oscillations might not have been observed yet in biological networks. This work also provides satisfaction

in building low-power, scalable devices that can integrate complex nervous stimuli to provide bioelectronic pacing for chronic disease [23,24] and brain-machine interfaces [25].

The paper is organized as follows. Section II describes the neuromorphic device and the method used to construct the state vector. We then classify the modes of synchronized oscillations according to their interspike interval and plot them in phase space. Section III reports on the stability of the coherent state as a function of inhibition delay and synaptic kinetics. We also report on the effect of inhibition delay, inhibition recovery time, and amplitude of the current stimulation on the phase maps of the four-neuron network. Section IV reports on the effect of network heterogeneity and additive noise on phase maps. Section V discusses the findings and concludes the paper.

II. EXPERIMENTAL MODEL AND METHOD

A. Neuromorphic central pattern generator

We built a neuromorphic network connecting each pair of neurons with mutually inhibitory synapses [Fig. 1(a)]. The device had 6 neurons and 36 synapses allowing for various network configurations to be studied [Fig. 1(b)].

The neurons modeled the Na, K, and leak channels (NaKIs) using discrete-component very large scale integration (VLSI) circuits implementing analog current mirrors [26]. For most practical purposes the circuit equations [24,27,28] are identical to those of the Hodgkin-Huxley model [29]. The two main differences are that the circuit does not replicate the exponents of gate variables in the Hodgkin-Huxley model, such as n^4 and m^3h . Secondly, the width of the transition region from the open to the closed state of a gate is identical for all ionic gates. This is set by the ratio of the oxide layer capacitance to the depletion region capacitance in our current mirrors, which is fixed by the technological process [24,30]. Each analog neuron has otherwise the same adjustable parameters as in the Hodgkin-Huxley model. This includes the ion channel conductances, the activation and inactivation voltage thresholds, and the gate recovery times. These parameters are set by the nine potentiometers of each neuron circuit [Fig. 1(b), green dashed box]. Our neurons had an oscillation threshold of $7 \mu\text{A}$, above which the oscillation frequency increased monotonically. For example, a current injection of $I_{\text{stim}} = 30 \mu\text{A}$ gave an oscillation period $T = 23 \text{ ms}$.

Our inhibitory synapses consisted of a differential pair integrator circuit [31] which injected a negative IPSC pulse following stimulation by a presynaptic action potential. The IPSC wave form was controlled by three parameters set by the three potentiometers seen in the synaptic circuit [Fig. 1(b), white dashed box]. The weight parameter sets the maximum synaptic conductance, \bar{g} . The integration time parameter set the decay time, τ , of the IPSC. The threshold parameter was used to retard the onset of the IPSC pulse by delay d relative to the depolarization of the presynaptic neuron.

In common with biological networks, our neuromorphic network is mildly heterogeneous. This has to be kept in mind when assessing the robustness of rhythmic patterns. Heterogeneity arises from component-to-component fluctuations within the manufacturer tolerances (5–10%), experimental error in setting neuron and synapse and parameters via potentiometers (5%). The analog circuit is also subject to time-dependent perturbations. These include intrinsic noise in the form of $1/f$ electronic noise (as in the nervous system) and Johnson noise. Our IPSCs carry an intrinsic noise $\sigma \approx 400 \text{ nA}$ when the typical IPSC pulse peaks at $12 \mu\text{A}$. Over long periods of time, thermal fluctuations also affect the transconductances of field effect transistors and can alter network properties when its dynamics is probed over hour-long experiments. In addition to these time-dependent perturbations, we are able to add white noise to current stimuli to study the stochastic response of the network.

B. State trajectories

Each neuron in the network was stimulated by current steps of equal amplitude I_{stim} [Fig. 1(a)] but variable timing. It was the timing of current stimuli that set the initial conditions of our network [Fig. 1(b)]. The current steps applied to neurons $n = 2, \dots, N$ were delayed by δt_n relative to the step applied to neuron 1 and varied in the interval $0 \leq \delta t_n \leq T$. We constructed the state vector (ϕ_2, \dots, ϕ_N) of the network by measuring the AP dephasings of neurons $2 \dots N$ relative to the AP of neuron 1 [15,32,33]. The state

trajectory was constructed by tracking the AP dephasings in each oscillation period from the first ($i = 1$) onwards ($i > 50$). For example, the dephasings (ϕ_2, ϕ_3, ϕ_4) of the four-neuron network in period $i = 4$ are shown in Fig. 1(c) for a given set of initial conditions. The trajectory of the state vector $[\phi_2(i), \phi_3(i), \phi_4(i)]$ was then plotted in phase space for $i = 1, 2, \dots, 50$ and orthographically projected in the plane [Fig. 1(d)].

In order to map the state trajectories emanating from initial conditions filling the entire phase space, we designed the following stimulation protocol. Current steps were synthesized by a pair of LABVIEW-controlled data acquisition (DAQ) cards (NI6259) and voltage-to-current converter electronics. The stimulation protocol consisted of 800-ms-long epochs in which the network oscillations were recorded in response to a given pattern of current steps. Each epoch was separated from the next by a 200-ms-long interval where no current stimulation was applied allowing the network to return to its quiescent state. The stimulation protocol of the next epoch was then applied, and the time series membrane voltage was recorded. The LABVIEW program varied the $\delta t_2, \dots, \delta t_N$ between 0 and T in raster scan fashion with a step size of $T/30$. For example, we recorded 27 000 sets of 800-ms-long network oscillations to map the dynamics of the four-neuron network.

A separate MATLAB program was written to analyze these recordings by detecting the timings of action potentials and computing their phase differences ϕ_2, \dots, ϕ_N over the first 50 oscillations of each epoch. The evolution of the state vector over each epoch was plotted as a state trajectory in phase space [Fig. 1(d)]. The trajectories constructed from all epochs mapped the entire phase space and hence the complete dynamics of the network. The trajectories converging to the same phase space coordinates to within $T/100$ were assigned the same color. This helped visualize attractors and their basins.

C. Phase coordinates of synchronized oscillations

The steady-state oscillations of inhibitory networks may be reliably classified according to the length of their interspike interval (ISI). Assuming an N -neuron network where S APs are coincident with some of the $N - S$ other APs, then the ISI is $T/(N - S)$. This ISI is a good invariant for homogeneous networks as states with the same ISI exhibit similar dynamics independently of the way in which the coincident APs are cyclically ordered. The four modes of synchronized oscillations in our four-neuron network are labeled $\text{ISI} = T/4, T/3, T/2, T/1$ [Fig. 2(a)]. The $\text{ISI} = T/4$ mode corresponds to the AP sequence 1234 and its five cyclically ordered permutations. The phase map coordinates of the corresponding attractor are $(1/4, 2/4, 3/4) + 5$ permutations [Fig. 2(b), black dots]. The $\text{ISI} = T/3$ mode has one coincident and three sequential APs that form the 12 following patterns: $\{12\}34$ at coordinates $(0, 1/3, 2/3) + 5$ permutations, $1\{23\}4$ at $(1/3, 1/3, 2/3) + 2$ permutations, and $12\{34\}$ at $(1/3, 2/3, 2/3) + 2$ permutations [Fig. 2(b), blue dots]. The $\text{ISI} = T/2$ mode has two coincident and two sequential APs distributed as $\{12\}\{34\}$ and $1\{234\}$ with attractors located at $(0, 1/2, 1/2) + 2$ permutations, $(0, 0, 1/2) + 2$ permutations, and $(1/2, 1/2, 1/2)$, respectively, giving

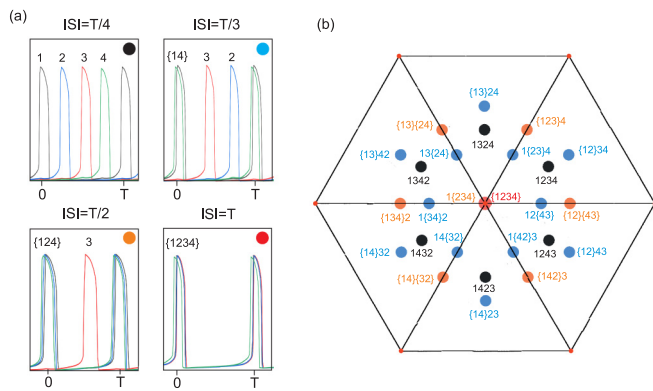


FIG. 2. Synchronized oscillation patterns of a four-neuron inhibitory network. (a) Synchronized modes of spatiotemporal oscillations ranging from sequentially discharging neurons ($ISI = T/4$), through partially coherent oscillations ($ISI = T/3, T/2$), to the fully coherent state where all neurons fire in phase ($ISI = T$). (b) Phase space coordinates of the stable modes of synchronized oscillations. Each node is labeled with its AP sequence. The curly brackets indicate neurons firing simultaneously. The colored dots correspond to the oscillation modes in (a).

seven attractors in total [Fig. 2(b), orange dots]. Finally, the $ISI = T/1$ mode has all four neurons firing in phase giving a single attractor at $(0,0,0)$. The maximum number of oscillations is therefore $T_4 = 6 + 12 + 7 + 1 = 26$. A combinatorial study allowing for the coincidence of APs has shown that a network of N all-to-all inhibitory neurons has a maximum of $T_N \sim (N - 1)!/\ln^N 2$ states [17].

III. RESULTS

A. d - T phase diagrams

We first probed the stability of the coherent state $ISI = T/1$ to generalize the criteria of synchronization, known from the mutually inhibitory neuron pair, to local inhibitory networks. White *et al.* [34], Van Vreeswijk *et al.* [22], Lewis and Rinzel [35], and Kopell and Ermentrout [36] have already established that phasic synchronization can be induced by certain values of the ratio T/τ . However, unlike in the mutually inhibitory neuron pair where synchronization is either phasic or antiphasic, local networks support a full spectrum of partially coherent oscillations in between, ranging from purely phasic to purely antiphase [Fig. 2(a)]. It is therefore relevant to ask whether the commensurability of T and τ still holds and what the phasic mode looks like: Is it a fully coherent or partially coherent state? In addition, we identify the inhibition delay d as a second important criterion of synchronization. This delay is the time interval between the onset of depolarization of the presynaptic neuron and the onset of the IPSC pulse. We find that when d is at least 30% of the AP duration ($d > 300 \mu s$), the network always supports fully coherent oscillations. This is true whether T and τ are commensurate or not. The commensurability of T and τ begins to play a role when $d < 300 \mu s$. The fully coherent state is then stabilized by making T and τ commensurate in the ratio $T/\tau \approx 14$. Otherwise, when $T/\tau \neq 14$, partially coherent oscillations replace the coherent state as the new stable states. As d decreases

below $d < 150 \mu s$ the fully coherent state vanishes to be replaced with partially coherent states at all values of the ratio T/τ . A difference between the mutually inhibitory pair ($N = 2$) and local inhibitory networks ($N > 2$) is that fully coherent oscillations are observed down to $d = 0$ in the former and down to a finite value of d in the latter ($d = 150 \mu s$ for $N = 4$).

We verified this in the phase diagrams of the four-neuron network showing the final state at the end of an 800-ms-long epoch [Figs. 3(a)–3(c)]. The network was initially prepared in its coherent state by four coincident current steps $\delta t_n = 0$, $n = 2, 3, 4$, and left to relax into its stable state. All synapses had the same nominal weight ($\bar{g} = 1.5 \mu S$). The final state is plotted as a function of inhibition delay d and I_{stim} . Increasing I_{stim} is equivalent to decreasing the oscillation period T . At $\tau = 1$ ms, we find that the fully synchronized state ($ISI = T/1$) is stable for long inhibition delays, $d > 300 \mu s$ (30% of the AP width), independently of the ratio T/τ [Fig. 3(a), yellow region]. Slowing synaptic recovery, from $\tau = 1$ ms [Fig. 3(a)] to 2 ms [Fig. 3(b)] and 3 ms [Fig. 3(c)] has the effect of shifting the coherent domain to larger values of T . The lowest point of the coherent domain, at $d \approx 150 \mu s$, occurs at a constant value of the ratio $T/\tau \approx 14$. When $d < 150 \mu s$, the coherent state vanishes and is replaced with partially coherent states ($ISI = T/3$).

These results are then compared with the phase diagram of the two-neuron network [Fig. 3(d)]. We similarly find that phasic oscillations occur at larger d albeit for $d > 225 \mu s$. This confirms that inhibition delay is a key criterion of synchronization. When $d < 225 \mu s$, phasic oscillations are only stabilized on the condition that the commensurability criterion $T/\tau \approx 19$ is satisfied. Elsewhere, synchronization is antiphase. The inhibitory pair, however, differs from the four-neuron network in that the coherent state is observed down to $d = 0$ provided the commensurability condition is satisfied. This is consistent with computational studies of pairs of inhibitory neurons [22,34]. The d -vs- T phase diagrams thus demonstrate that phasic oscillations can be stabilized in two ways: (i) through delayed inhibition and (ii) at specific ratios of T/τ [28].

We now map the complete network dynamics of the four-neuron network by varying initial conditions. The aim is to identify the full complement of limit cycles and to study their dependence on parameters d , T , and I_{stim} .

B. Inhibition delay stabilizes coincident APs

Figure 4(a) shows the effect of increasing inhibition delay on the IPSC pulse as d increases from 40 to 320 μs . All 12 synapses were configured with the same nominal d , $\tau = 1$ ms, and $\bar{g} = 1.5 \mu S$. When $d < 100 \mu s$, the network hosts six attractors corresponding to the six sequential discharge patterns of the four neurons [Fig. 4(b)]. These states represent the limit cycles of winnerless networks [18] with wide basins of attraction (black lines). Increasing inhibition delay to $d = 220 \mu s$ [Fig. 4(c)] introduces 12 new basins of attraction (blue lines) centered on the theoretical coordinates of the $\{12\}34$ patterns with $ISI = T/3$. Further increase in inhibition delay to $d = 320 \mu s$ [Fig. 4(d)] stabilizes the seven partially coherent oscillations with $ISI = T/2$ (orange lines) and the lone

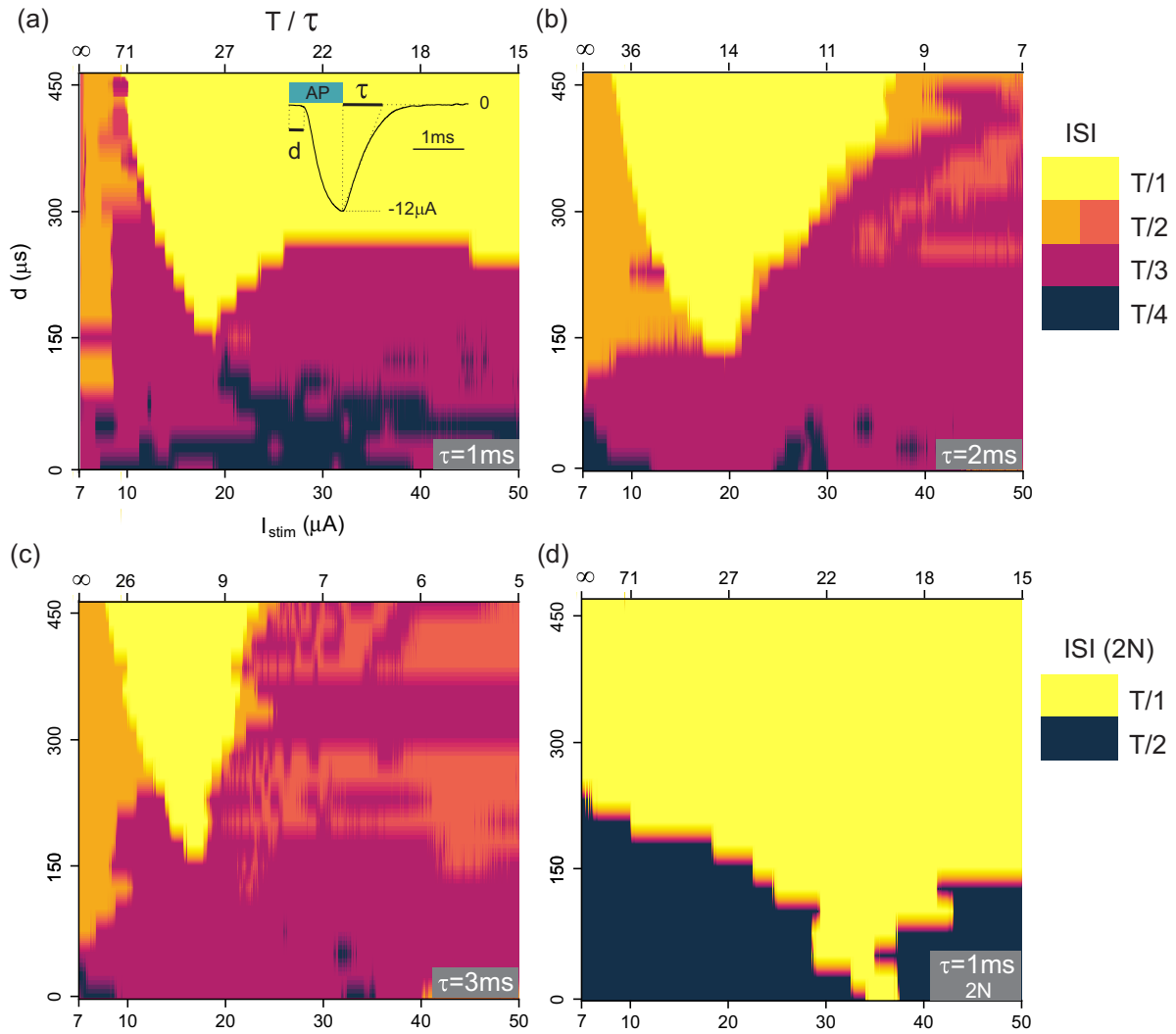


FIG. 3. d - T phase diagrams of four-neuron and two-neuron inhibitory networks. (a) Phase diagram of the four-neuron network plotting the final state of the network with ISI $T/1$ (yellow), $T/2$ (orange), $T/3$ (pink), or $T/4$ (black) after the network has been stimulated with synchronous current pulses ($\delta t_i = 0$) of equal amplitude ($I_{stim} = 32 \mu A$). The phase diagrams show the dependence of the final state as a function of inhibition delay d and the amplitude of current steps I_{stim} . The oscillation period T is plotted on the top axis in units of the synaptic recovery time τ . Here, $\tau = 1$ ms. Inset: IPSC wave form showing the parameters being varied: inhibition delay d , synaptic recovery time τ , and IPSC amplitude $12 \mu A$. (b) $\tau = 2$ ms. (c) $\tau = 3$ ms. (d) Phase diagram of a mutually inhibitory neuron pair for $\tau = 1$ ms.

coherent state with ISI = $T/1$ (red lines). Inhibition delay thus increases the number of attractors by allowing coincident APs in the cyclical discharge patterns of the network. The larger the delay, the greater the coherence of oscillatory patterns. These experiments show that a physical network holds up to 26 oscillatory patterns, which is the combinatorially predicted number of activation pathways in a four-neuron network. Note that the hardware supports all these oscillations despite mild network heterogeneity and electronic noise.

IPSCs act as a repulsive force between action potentials. The effect of inhibition delay is to open a time window during which the repulsion between coincident spikes is switched off. If this window is sufficiently long, depolarization will be initiated before inhibition from the antagonist neuron is received. The larger the time window, the longer the transmission delays it can accommodate. This allows next-nearest-neighbor neurons to fire in phase with the inhibitory pair producing larger and larger clusters of coincident action potentials as d

increases. Even in local networks with small transmission line delays, inhibition delays a few hundred microseconds long are sufficient to stabilize coherent oscillations. Inhibition delay constitutes one criterion for phasic synchronization. The other criterion is the commensurability of T and τ [28,34] as we now show by varying τ .

C. τ increases network stiffness

Figure 5(a) shows the IPSC pulses measured for different synaptic recovery times, ranging from $\tau = 1$ ms to $\tau = 4$ ms. All synapses were configured with the same nominal $d = 250 \mu s$, τ , and $\bar{g} = 1.5 \mu S$. Increasing τ has the effect of increasing the repulsive force between action potentials. As the network connectivity becomes stiffer, the network adjusts faster to stimuli. This is seen in the narrowing of the basins of sequential modes [Figs. 5(b)–5(d), black lines] as state trajectories converge faster to their attractor. In contrast, the

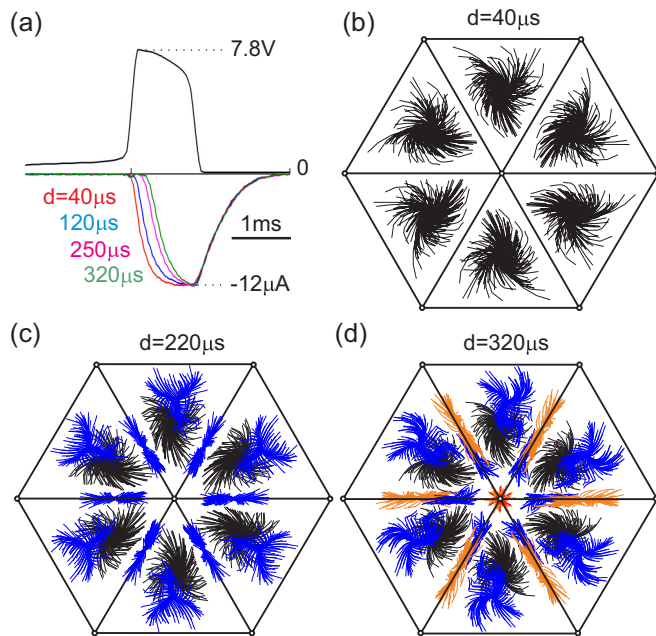


FIG. 4. Effect of increasing inhibition delay on phase maps. (a) IPSC wave forms (colored lines) delayed relative to the presynaptic action potential (black line) with delays $d = 40\text{--}320 \mu\text{s}$. (b)–(d) Phase lag maps of the four-neuron inhibitory network at increasing inhibition delay: (b) $d = 40 \mu\text{s}$, (c) $d = 220 \mu\text{s}$, and (d) $d = 320 \mu\text{s}$. State trajectories converge to attractors with $\text{ISI} = T/4$ (black lines), $T/3$ (blue lines), $T/2$ (orange lines), and $T/1$ (red lines) from different initial states. Parameters: $\tau = 1 \text{ ms}$, $\bar{g} = 1.5 \mu\text{S}$, $I_{\text{stim}} = 30 \mu\text{A}$.

basins of partially coherent states widen. This increase is most significant in the $\{12\}34$ modes (blue lines) and less pronounced in the $\{123\}4$ and $\{1234\}$ modes (orange and red lines, respectively). In addition, increasing τ shifts the attractors of the $\{12\}34$ modes towards the outer vertices of the map [Fig. 5(d)], whereas the attractors of the more coherent modes, $\{123\}4$ and $\{1234\}$, stay at the same location. This occurs as longer inhibition delays allow a residual phase shift between coincident action potentials. This shift introduces ISIs of uneven duration in the $\{12\}34$ sequence and hence a shift in attractor coordinates. The same inhibition delay gives a smaller shift in the $\{123\}4$ and $\{1234\}$ sequences as it is distributed among three and four coincident APs. As τ increases from 1 to 3 ms, the ratio T/τ approaches the optimum ratio that stabilizes phasic oscillations ($\{1234\}$). In our next experiment, we systematically vary T to demonstrate the commensurability of T and τ as our second criterion of synchronization.

D. Commensurability of T and τ stabilizes coincident APs

Figure 6(a) plots the experimental dependency of the oscillation period T on I_{stim} . All synapses were configured with the same nominal $d = 250 \mu\text{s}$, $\tau = 2 \text{ ms}$, and $\bar{g} = 1.5 \mu\text{S}$. We increased current stimulation from $I_{\text{stim}} = 20 \mu\text{A}$ to $I_{\text{stim}} = 46 \mu\text{A}$ to vary the ratio T/τ from 14 (commensurability condition) to 8 [Figs. 6(b)–6(d)]. In Fig. 3(b), this is equivalent to moving along the horizontal line $d = 250 \mu\text{s}$, from $T/\tau = 14$

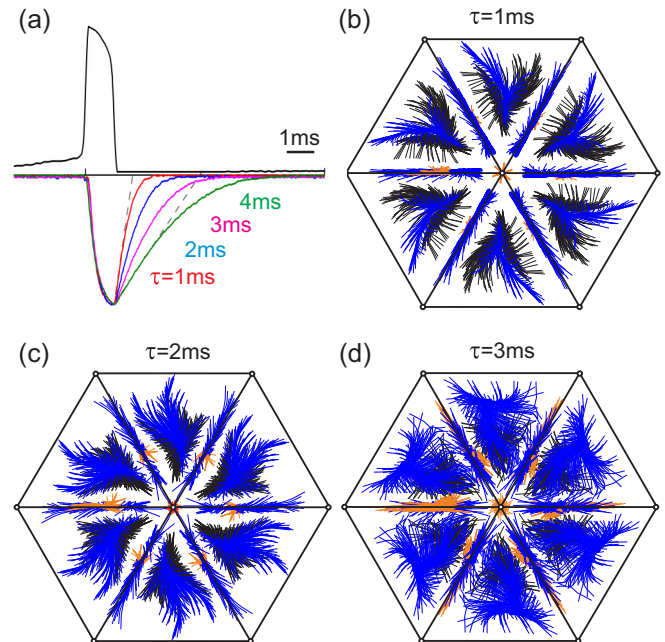


FIG. 5. Effect of increasing the synaptic recovery time. (a) IPSC wave forms measured at different synaptic recovery times $\tau = 1\text{--}4 \text{ ms}$ (colored lines). Phase lag map of the four-neuron inhibitory network recorded at three values of the recovery time: (a) $\tau = 1 \text{ ms}$, (b) $\tau = 2 \text{ ms}$, and (c) $\tau = 3 \text{ ms}$. State trajectories converge to attractors with $\text{ISI} = T/4$ (black lines), $T/3$ (blue lines), $T/2$ (orange lines), and $T/1$ (red lines). Parameters: $d = 250 \mu\text{s}$, $\bar{g} = 1.5 \mu\text{S}$, $I_{\text{stim}} = 30 \mu\text{A}$.

where the coherent state ($\text{ISI} = T/1$) is stable to 8 where states $T/3$ and $T/4$ are stable. This transition is shown in the phase lag maps of Figs. 6(b)–6(d), which plot state trajectories starting from all initial conditions rather than from the coherent state only (Fig. 3). We find that of the 26 attractors initially observed at $T/\tau = 14$ [Fig. 6(b)] only 18 survive at $T/\tau = 8$ [Fig. 6(d)]. These are the least coherent states with $\text{ISI} = T/3$ and $T/4$. The commensurability of T and τ therefore allows local networks to support *all* attractors simultaneously, ranging from purely phasic to purely antiphase. Moving away from the commensurability condition suppresses the coherent modes leaving increasingly antiphase oscillations as the stable states. Our experiment thus provides nuance and expands earlier findings on mutually inhibitory neuron pairs where the commensurability of T and τ was associated with purely phasic synchronization only [22].

IV. STABILITY OF SPATIOTEMPORAL OSCILLATIONS

A. Sparser connectivity

We have so far studied mildly heterogeneous networks with nominally identical synapses to demonstrate the maximum number of attractors supported by the network. Increasing network heterogeneity will eventually reduce this number by allowing the fastest neurons to switch off the slower neurons. Before this situation occurs, heterogeneity is expected to introduce ISIs of uneven duration and hence shift the position of attractors in phase maps [33]. Here, we investigate

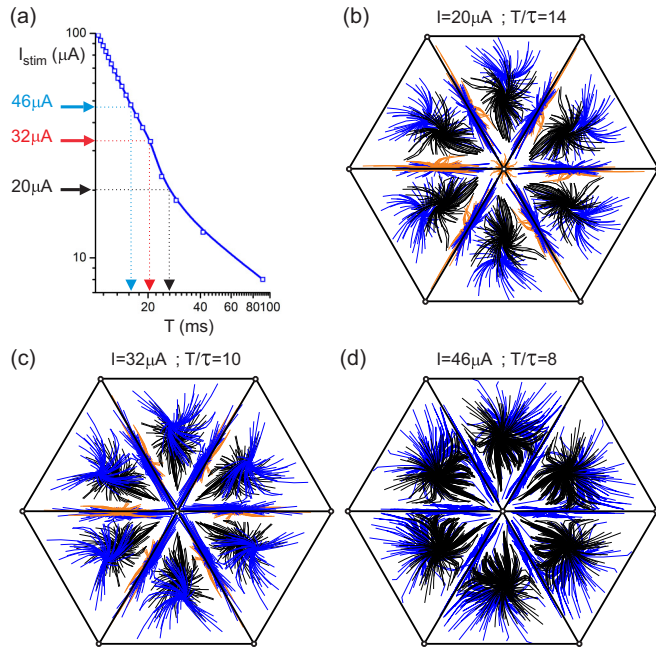


FIG. 6. Effect of increasing neuron stimulation. (a) Empirical relationship between the amplitude of tonic current stimulation, I_{stim} , and the period of network oscillations T . Phase lag map of the four-neuron inhibitory network recorded at three current values: (a) $I_{stim} = 20 \mu A$ ($T = 27 ms$), (b) $I_{stim} = 32 \mu A$ ($T = 20.5 ms$), and (c) $I_{stim} = 46 \mu A$ ($T = 16 ms$). State trajectories converge to attractors with ISI = $T/4$ (black lines), $T/3$ (blue lines), $T/2$ (orange lines), and $T/1$ (red lines). Parameters: $d = 250 \mu s$, $\tau = 1 ms$, $\bar{g} = 1.5 \mu S$.

whether this theoretically predicted shift actually occurs in physical networks. We also seek to establish the one-to-one correspondence between limit cycles and activation pathways which underpins our calculation of the maximum number of attractors. We do this by switching off selected pathways. We then examine the network dynamics in the vicinity of ghost attractors corresponding to the suppressed pathways [37–39].

In both cases we find significant departures from theory. Although each attractor does relate to an activation pathway, their maximum number was found to be surprisingly robust against network heterogeneity. Secondly, trajectories in the vicinity of ghost attractors are found to diverge rather than converge towards the remaining attractor(s) [33].

We start from the balanced inhibitory network of Fig. 4(b) and progressively decrease the conductances of the inner synapses while leaving the four clockwise projecting conductances equal to $\bar{g}_{12} = \bar{g}_{23} = \bar{g}_{34} = \bar{g}_{41} = 1.5 \mu S$ (Fig. 7). Without loss of generality, we studied the effect of heterogeneity on the six sequential oscillations only [Fig. 7(a)]. Halving the inner conductances from $1.5 \mu S$ to $0.75 \mu S$ introduces cycle-to-cycle variability in the timing of APs, which translates into more erratic trajectories [Fig. 7(b)]. Surprisingly, the basin size of the 1234 sequence does not grow relative to the five other basins. Instead, all six basins remain equivalent in size. This is unlike simulations predicting the expansion of the 1234 basin [33,40]. The picture that emerges from experimental networks is that the timing of an action potential is not determined by only the IPSC from the last firing neuron in the sequence but rather by all neurons. For example, in the 1234 sequence, neuron 2 is inhibited by neuron 1 ($\bar{g}_{12} = 1.5 \mu S$) and by neurons 3 and 4 ($\bar{g}_{32} = \bar{g}_{42} = 0.75 \mu S$). The IPSC from the last neuron firing in the sequence (neuron 1) is modulated by the periodic subthreshold oscillations of all other neurons, which may be transmitted through synapses through stochastic processes. The entrainment by subthreshold neurons is believed to stabilize the six activation pathways, in particular those with weaker links. This resilience of network oscillations to heterogeneity is finally broken when the inner conductances are set to zero [Fig. 7(c)]. A single attractor remains which corresponds to the 1234 sequence. The state trajectories emanating from the five former basins thread the entire phase space without converging suggesting asynchronous network oscillations.

These results thus demonstrate the correspondence between a limit cycle and a path of propagation of electrical activity. This explains that the total number of attractors is

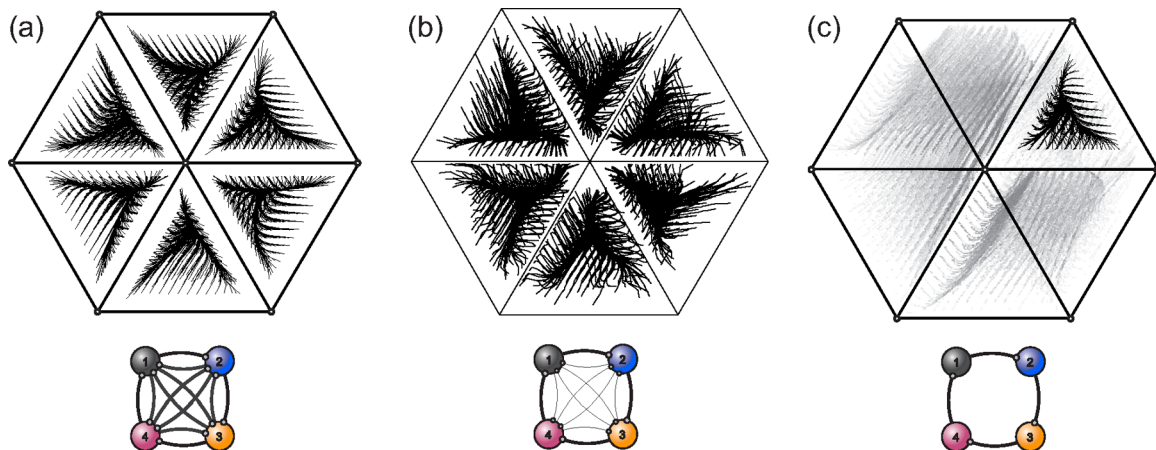


FIG. 7. From all-to-all to ringlike connectivity. Effect of introducing sparser network connectivity on the phase lag maps. (a) All-to-all inhibitory network: All synapses are nominally identical with $\bar{g}_{n \neq m} = 1.5 \mu S$, $d = 40 \mu s$, and $\tau = 1 ms$. (b) Unbalanced network: Synaptic strengths are halved to $\bar{g}_{n \neq m} = 0.75 \mu S$ except for along the outer ring, where $\bar{g}_{12} = \bar{g}_{23} = \bar{g}_{34} = \bar{g}_{41} = 1.5 \mu S$. (c) Clockwise projecting oscillator ring: $\bar{g}_{n \neq m} = 0$ except along the outer ring, where $\bar{g}_{12} = \bar{g}_{23} = \bar{g}_{34} = \bar{g}_{41} = 1.5 \mu S$.

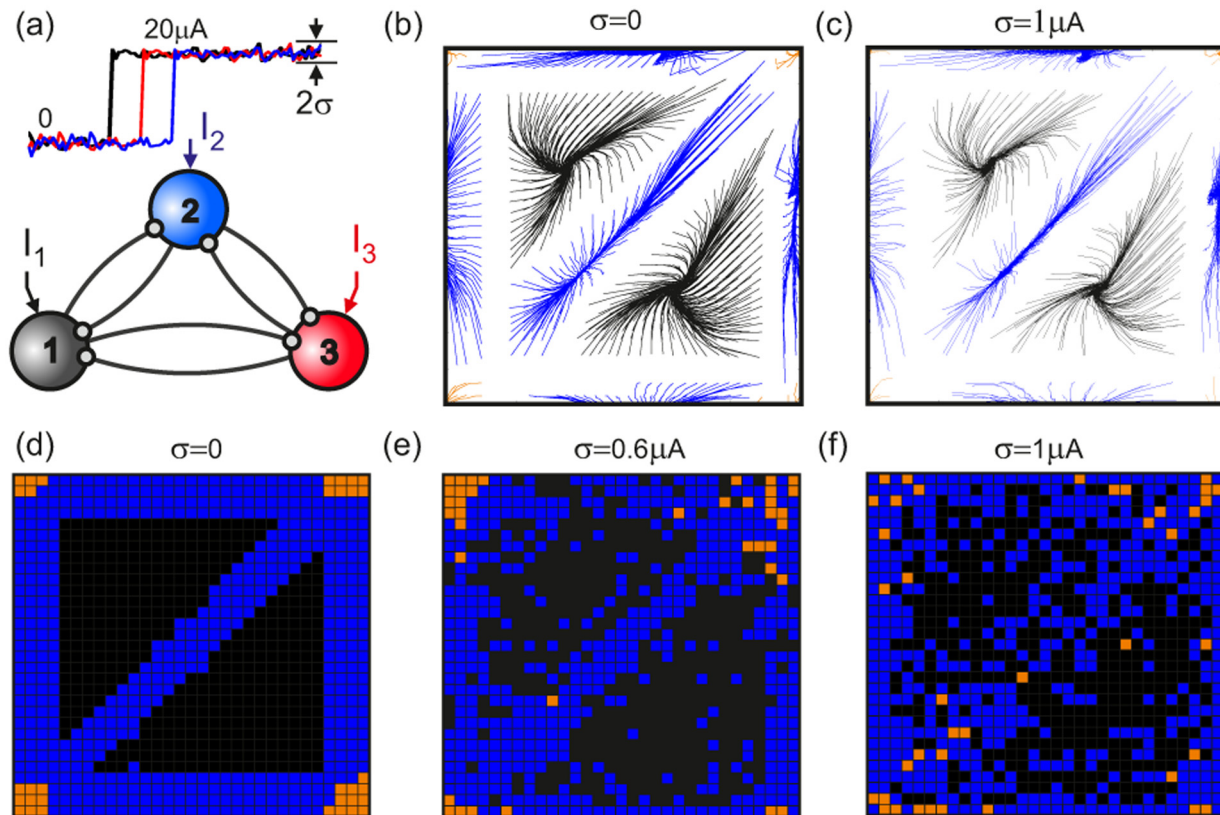


FIG. 8. Effect of extrinsic noise on network dynamics. (a) Three-neuron inhibitory network stimulated by timed current steps ($20 \mu\text{A}$) superimposed with Gaussian noise $\sigma = 0\text{--}1 \mu\text{A}$. Inhibition delay $d = 300 \text{ ms}$ stabilizes all six limit cycles. Phase lag maps for (b) $\sigma = 0$ and (c) $\sigma = 1 \mu\text{A}$ show the state trajectories staying in the same basin of attraction. (d)–(f) Pixel maps visualizing noise-induced switching between basins. The pixel color indicates the basin of origin. The pixel coordinates indicate the end state after 50 cycles. $\text{ISI} = T/4$ (black), $T/3$ (blue), $T/2$ (orange), $T/1$ (red). (d) $\sigma = 0$, (e) $\sigma = 0.6 \mu\text{A}$, and (f) $\sigma = 1 \mu\text{A}$. Parameters: $\tau = 1 \text{ ms}$, $I_{\text{stim}} = 20 \mu\text{A}$, $\bar{g} = 1.5 \mu\text{S}$.

equal to the combinatorial number of such pathways: $T_N \sim (N - 1)!/\ln^N 2$ when allowing coincident APs and $R_N = (N - 1)!$ otherwise [17]. In contrast to simulations of noise-free networks, all neurons are found to entrain the firing neuron and not just the last neuron(s) in the sequence. This contribution from the whole network has the effect of stabilizing all attractors against heterogeneity, giving six basins of similar size.

B. Extrinsic noise

Local networks receive noisy stimuli through afferent synapses. This noise tends to arise from the quantal release of calcium from synaptic vesicles and neurotransmitter release. We simulated this extrinsic noise and its effect on the network dynamics by adding Gaussian noise to current steps $I_i(t) + \zeta(t)$, where the noise time series ζ follows a normal distribution $\mathcal{N}(0, \sigma)$ with standard deviation σ [Fig. 8(a)]. We tuned σ between 0 and $1 \mu\text{A}$.

For clarity, we begin by investigating the effects of noise on a three-neuron network with all-to-all connectivity. This network has six oscillatory modes [Fig. 8(b)]: Two sequential modes 123 with $\text{ISI} = T/3$ (black lines), three partially synchronized modes $\{12\}3$ with $\text{ISI} = T/2$ (blue lines), and one coherent state $\{123\}$ with $\text{ISI} = T/1$ (orange lines). Noisy stimuli add random phase shifts to action potentials. This

perturbation of state trajectories is seen in Fig. 8(c). Quite remarkably, all six attractors survive at a noise level of $\sigma = 1 \mu\text{A}$. This verifies the predicted robustness of sequential oscillations [18] and generalizes the claim to limit cycles allowing coincident action potentials.

Noise also induces switching between attraction basins. We visualize this in a pixel array encoding the basin of origin in the pixel color and the end state of the trajectory in the coordinates of the pixel [Fig. 8(d)]. As the noise amplitude increases from 0 to $\sigma = 0.6 \mu\text{A}$ [Fig. 8(e)] and $\sigma = 1 \mu\text{A}$ [Fig. 8(f)], state trajectories diffuse into vicinal basins. The net number of trajectories switching out a basin minus the incoming trajectories remains approximately constant independently of the size of the basin (i.e., $\text{ISI} = T/1, T/2$, or $T/3$) and the noise level.

This observation is confirmed by further experiments on the four-neuron network (Fig. 9) which yield the detailed balance of transitions between basins as a function of noise. Transition probabilities were calculated from a statistical sample of initial conditions uniformly distributed over the entire phase space. The colored bands in Fig. 9 shows the probability of a trajectory ending in one of the four oscillatory modes with $\text{ISI} = T/1, T/2, T/3$, or $T/4$. The hatch pattern within each colored band indicates the initial oscillatory mode. The constant width of each colored band as noise amplitude increases shows that each mode attracts the same fraction of

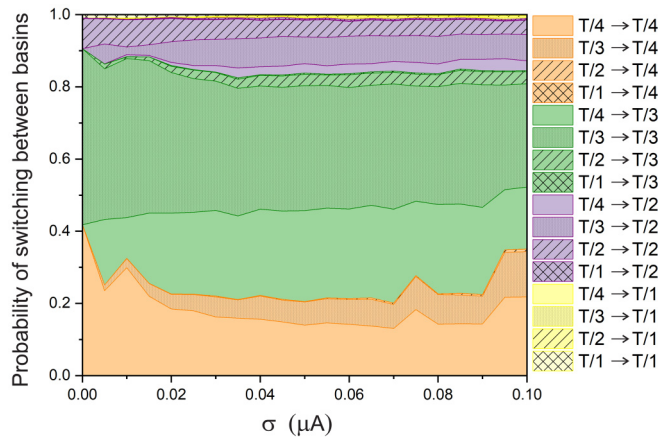


FIG. 9. Noise-induced switching probability between basins. Cumulative switching probability between the basins of a four-neuron network as a function of noise amplitude σ .

trajectories independently of the noise level. In particular, the phasic state (yellow band) captures the same fraction of trajectories independently of the noise level, and this is in spite of this state having the smallest basin size. Within each colored band, noise increases the probability of switching out of the original mode; however, this is almost exactly compensated by the number of trajectories coming in from the other basins. This experiment displays two opposite effects of noise on the network dynamics. Noise accelerates the convergence of vicinal trajectories towards limit cycles by introducing negative Lyapunov exponents [32]. However, noise also randomizes the phase of neuron oscillations. This can propel transitions between basins especially for trajectories passing near saddle points [41,42]. The lack of noise dependence in the transition probabilities into an oscillatory mode (Figs. 8 and 9) is likely to arise from the compensation of the randomizing and stabilizing effects of noise.

V. DISCUSSION

If the oscillatory states predicted by combinatorics are robust against temporal and spatial fluctuations, why is it that only a tiny fraction of the maximum possible number is observed in the brain?

One possibility is that all-to-all inhibition is realized in small networks within the radius of the axon, on a scale too small to be accessible to observation. Relevant inhibitory networks include the basket cells in the hippocampus, thalamus, olfactory bulb, and neocortex [43] and pairs of recurrent inhibitory neurons which underpin the rhythmic oscillation of central pattern generators [12,44]. Modern functional imaging techniques, such as multichannel electroencephalography, can only resolve electrical activity at the level of brain lobes to ≈ 20 mm [45]. *In vivo* imaging of the electrical activity of individual neurons would require a resolution better than 3 mm. Equally, it remains challenging to isolate and preserve functional networks in brain slices for performing electrophysiological measurements. It is therefore possible that the states we report may exist but are not yet accessible to current experimental techniques.

Secondly, asynchronous stimuli are required to activate the full spectrum of oscillations supported by inhibitory networks. Earlier simulations of Γ and θ brain waves have not systematically varied the timing of initial conditions [2,7,34,46], instead focusing on initiating network oscillations with synchronous current pulses of random amplitude [9,36]. Kopell and Ermentrout [36] report that inhibitory networks erase the memory of initial conditions. This is indeed the case in our experiments when state trajectories propagate from initial conditions to the final limit cycle in Figs. 4–6. In order to evoke the combinatorially predicted oscillations, however, the timing of current stimuli must be varied over the entire phase space. If, instead, the network is stimulated with synchronous current steps of random amplitude, the initial state will always be the coherent state, which may then decay into one of the four possible oscillator modes as demonstrated in Fig. 3. Hence synchronous stimuli could evoke no more than a few of the combinatorially predicted states we report here.

We found that the maximum number of oscillations may be stabilized in two ways, either through delayed inhibition or at specific values of the ratio of the oscillation period to the synaptic recovery time ($T/\tau \approx 14$). The commensurability mechanism is well known [21,34,46,47] in fast-spiking neurons [4], and it is exploited in the design of antiepileptic drugs that alter synaptic kinetics by targeting GABA receptors [2]. The role of transmission line delay in delaying inhibition has been recognized more recently [14,28,48,49]. Delayed inhibition may be exploited by somatostatin neurons [5] to promote visual binding. These neurons project to the dendrites of postsynaptic neurons, which allows transmission line delays of $d = 60$ – 800 μ s from the onset of the presynaptic action potential to the onset of depolarization of the postsynaptic neuron [50]. Our work has expanded on these synchronization criteria from pairs of inhibitory neurons [22,51] to three- and four-neuron networks and from stimuli of variable amplitude to variable timings. We have shown that coherent oscillations can only exist in local networks with a finite inhibition delay: $d > 150$ μ s [Figs. 3(a)–3(c)]. This is unlike the inhibitory neuron pair, where phasic oscillations are observed down to $d = 0$ [Fig. 3(d)]. In networks of any size, coherent oscillations are most stable when $T/\tau \approx 14$. It is, however, the length of inhibition delay which determines the maximum number of oscillations. Increasing d from 0 to over 250 μ s increases the maximum number of oscillations from $R_4 = 6$ to $T_4 = 26$ in the four-neuron network (Fig. 3) and from $R_3 = 2$ to $T_3 = 6$ in the three-neuron network [Fig. 8(b)]. The combinatorially predicted states are $R_N = (N - 1)!$ and $T_N = (N - 1)!/\ln^N 2$, respectively, in networks of N neurons [17].

Our results demonstrate the robustness of the combinatorially predicted oscillations to noise, both intrinsic (Figs. 3–6) and extrinsic (Figs. 8 and 9). The intrinsic noise in our device has the same $1/f$ electronic spectrum and thermal spectrum as in the brain with a signal-to-noise ratio of 20–30. Both intrinsic and extrinsic noise is expected to stochastically enhance transmission subthreshold signals. Weak noise levels stabilize periodic oscillations in the vicinity of limit cycles by introducing negative Lyapunov exponents [18–20,32,42,48,49]. At higher levels, noise randomly shifts the phase of APs, which may propel transitions between basins [41,52] and bifurcations [53]. There is a critical noise level above which

the smallest Lyapunov exponent of the system changes sign, going from negative to positive, making state trajectories diverge [20,52]. This critical noise level varies with position in phase space, depending on the closeness of a trajectory to a limit cycle or a saddle. Analytical and computational studies nearly always treat stochastic processes in the vicinity of special points [54] or through approximations, for example, by differentiating slow and fast state variables [53]. Our experiment instead computes the detailed balance of all transitions between attractors over the entire phase space. No prior assumption or approximation is made. We conclude that the fraction of trajectories ending in a given oscillatory mode is independent of the noise level. The transitions out of a basin are almost exactly compensated by the incoming transitions, the net effect being that no limit cycle is washed out by noise. Limit cycles with different degrees of coherence are robust to noise. This confirms and generalizes the predictions made for winnerless networks to networks supporting coincident APs [18].

Our results also demonstrate the robustness of the combinatorially predicted oscillations to mild network heterogeneity. Here, heterogeneity is both device specific and tuned by synaptic strengths (Fig. 7). Heterogeneity destroys synchronization by reducing the number of pathways for the electrical activity to bounce across. We have verified this in Fig. 7(c), where the action of suppressing physical pathways switches off limit cycles. We find, however, that the network is resilient to this trend and succeeds in preserving all limit cycles in the presence of mild heterogeneity. Figure 7(b) shows that *all* basins remain equal in size even after many synaptic conductances are halved. To achieve this, the network uses the additional synchronizing effect of the periodic oscillations of subthreshold neurons. At any given time these neurons generate IPSCs which modulate the IPSC of the last firing neuron. The larger the network, the larger these synchronizing contributions. Intrinsic noise in our network will enhance the transmission of these subthreshold oscillations through synapses [55–57]. Simulations by Wojcik *et al.* [14] consider the case of noiseless networks with all-or-nothing (± 1 mV) synaptic transmission in which the last firing neuron in the sequence generates an IPSC. In such a network, the electrical activity passes from one neuron to the next, without the background modulation and stabilizing effect of the entire network. We therefore suggest that the limit cycles of inhibitory networks might be more resilient to mild heterogeneity than hitherto anticipated from computer simulations due to the stochastic entrainment of the entire network.

Computation by neuromorphic hardware simulates the brain's noisy environment and heterogeneity while granting excellent control of network parameters. The ability of our analog network to integrate complex stimuli instantaneously has greatly facilitated our systematic study. The sensitivity of rhythmic patterns to initial conditions underlines the importance of control neurons and sensory inputs [58], which together with neuromodulation [13,59,60] determine the type of oscillations of the network. Neuromorphic devices are extremely power efficient [61,62] and are beginning to be used in bioelectronic medicine [24,63] and brain interfaces [64]. The possibility of activating multiple rhythmic patterns within the same local network is certainly very attractive for brain-machine interfaces [25].

VI. CONCLUSIONS

Our experiments on neuromorphic hardware have shown that local inhibitory networks support a very large number of oscillatory states, $\sim(N-1)!/\ln^N 2$. These states are activated by the specific timings of external stimuli and are very robust to network heterogeneity, intrinsic and extrinsic noise. It is therefore expected that these states may eventually be observed in functional biological networks as imaging techniques increase in resolution. Our findings modify the established picture of oscillatory modes in dynamic networks in two ways. Oscillatory patterns will generally include both sequential and coincident action potentials. The mechanisms enabling coincident action potentials are the inhibition delay and the commensurability of the synaptic recovery time to the period of network oscillations. Secondly, while we demonstrate the one-to-one correspondence between activation pathways in the network and oscillatory modes, we emphasize that at any given time *all neurons* contribute to a given oscillatory pattern through their subthreshold oscillations. This contribution from the wider network has not been recognized; however, we find it plays an important role in stabilizing oscillatory states against network heterogeneity.

ACKNOWLEDGMENTS

This work was supported by the European Union's Horizon 2020 Future Emerging Technologies Programme (Grant No. 732170). J.D.T. acknowledges support from the EPSRC (United Kingdom) for a doctoral studentship.

-
- [1] J. E. Lisman and O. Jensen, The theta-gamma neural code, *Neuron* **77**, 1002 (2013).
 - [2] M. A. Whittington, R. D. Traub, and J. G. Jefferys, Synchronized oscillations in interneuron networks driven by metabotropic glutamate receptor activation, *Nature (London)* **373**, 612 (1995).
 - [3] V. S. Sohal, F. Zhang, O. Yizhar, and K. Deisseroth, Parvalbumin neurons and gamma rhythms enhance cortical circuit performance, *Nature (London)* **459**, 698 (2009).
 - [4] J. A. Cardin, M. Carlén, K. Meletis, U. Knoblich, F. Zhang, K. Deisseroth, L.-H. Tsai, and C. I. Moore, Driving fast-spiking cells induces gamma rhythm and controls sensory responses, *Nature (London)* **459**, 663 (2009).
 - [5] J. Veit, R. Hakim, M. P. Jari, T. J. Sejnowski, and H. Adesnik, Cortical gamma band synchronization through somatostatin interneurons, *Nat. Neurosci.* **20**, 951 (2017).
 - [6] P. Tiesinga and T. J. Sejnowski, Cortical enlightenment: are attentional gamma oscillations driven by ING or PING? *Neuron* **63**, 727 (2009).

- [7] Z. W. Davis, L. Muller, J. Martinez-Trujillo, T. Sejnowski, and J. H. Reynolds, Spontaneous travelling cortical waves gate perception in behaving primates, *Nature (London)* **587**, 432 (2020).
- [8] M. M. Huntsman, D. M. Porcello, G. E. Homanics, T. M. DeLoery, and J. R. Huguenard, Reciprocal inhibitory connections and network synchrony in the mammalian thalamus, *Science* **283**, 541 (1999).
- [9] A. Destexhe, D. Contreras, T. J. Sejnowski, and M. Steriade, A model of spindle rhythmicity in the isolated thalamic reticular nucleus, *J. Neurophysiol.* **72**, 803 (1994).
- [10] S. O. Jeong, T. W. Ko, and H. T. Moon, Time-Delayed Spatial Patterns in a Two-Dimensional Array of Coupled Oscillators, *Phys. Rev. Lett.* **89**, 154104 (2002).
- [11] P. A. Getting, A network oscillator underlying swimming in *Tritonia*, in *Neuronal and Cellular Oscillators* (Dekker, New York, 1989), pp. 215–236.
- [12] J. Jing and R. Gillette, Central pattern generator for escape mechanism in the notaspidean sea slug: *Pleurobranchia californica*, *J. Neurophysiol.* **81**, 654 (1999).
- [13] A. Berkowitz, A. Roberts, and S. R. Ioffe, Roles for multifunctional and specialized spinal interneurons during motor pattern generation in tadpoles, zebrafish larvae and turtles, *Front. Behav. Neurosci.* **4**, 36 (2010).
- [14] J. Wojcik, J. Schwabedal, R. Clewley, and A. Shilnikov, Key bifurcations of bursting polyrhythms in 3-cell central pattern generators, *PLoS One* **9**, e92918 (2014).
- [15] C. C. Canavier, D. A. Baxter, J. W. Clark, and J. H. Byrne, Control of multistability in ring circuits of oscillators, *Biol. Cybern.* **80**, 87 (1992).
- [16] S. Achuthan and C. C. Canavier, Phase-resetting curves determine synchronization, phase-locking, and clustering in networks of neural oscillators, *J. Neurosci.* **29**, 5218 (2009).
- [17] A. Nogaret and A. King, Inhibition delay increases neural network capacity through Stirling transform, *Phys. Rev. E* **97**, 030301(R) (2018).
- [18] M. Rabinovich, A. Volkovskii, R. Lecanda, R. Huerta, H. D. I. Abarbanel, and G. Laurent, Dynamical Encoding by Networks of Competing Neuron Groups: Winnerless Competition, *Phys. Rev. Lett.* **87**, 068102 (2001).
- [19] Z. F. Mainen and T. J. Sejnowski, Reliability of spike timing in neocortical neurons, *Science* **268**, 1503 (1995).
- [20] D. S. Goldobin and A. Pikovsky, Synchronization and desynchronization of self-sustained oscillators by common noise, *Phys. Rev. E* **71**, 045201(R) (2005).
- [21] X.-J. Wang and G. Buzsáki, Gamma oscillations by synaptic inhibition in a hippocampal interneuronal network model, *J. Neurosci.* **16**, 6402 (1996).
- [22] C. Van Vreeswijk, L. F. Abbott, and G. B. Ermentrout, When inhibition not excitation synchronizes neural firing, *J. Comput. Neurosci.* **1**, 313 (1994).
- [23] E. L. O’Callaghan, R. M. Lataro, E. L. Roloff, A. S. Chauhan, H. C. Salgado, E. Duncan, A. Nogaret, and J. F. R. Paton, Enhancing respiratory sinus arrhythmia increases cardiac output in rats with left ventricular dysfunction, *J. Physiol.* **598**, 455 (2020).
- [24] K. Abu-Hassan, J. D. Taylor, P. G. Morris, E. Donati, Z. A. Bortolotto, G. Indiveri, J. F. R. Paton, and A. Nogaret, Optimal solid state neurons, *Nat. Commun.* **10**, 5309 (2019).
- [25] C. T. Moritz, S. I. Perlmutter, and E. E. Fetz, Direct control of paralysed muscles by cortical neurons, *Nature (London)* **456**, 639 (2008).
- [26] M. Mahowald and R. Douglas, A silicon neuron, *Nature (London)* **354**, 515 (1991).
- [27] L. Zhao and A. Nogaret, Experimental observation of multistability and dynamic attractors in silicon central pattern generators, *Phys. Rev. E* **92**, 052910 (2015).
- [28] A. S. Chauhan, J. D. Taylor, and A. Nogaret, Dual mechanism for the emergence of synchronization in inhibitory neural networks, *Sci. Rep.* **8**, 11431 (2018).
- [29] A. L. Hodgkin and A. F. Huxley, A quantitative description of membrane current and its application to conduction and excitation nerve, *J. Physiol.* **117**, 500 (1952).
- [30] J. Wang, D. Breen, A. Akinin, F. Broccard, and H. D. I. Abarbanel, Assimilation of biophysical neuronal dynamics in neuromorphic VLSI, *IEEE Trans. Biomed. Circuits Syst.* **11**, 1258 (2017).
- [31] C. Bartolozzi and G. Indiveri, Synaptic dynamics in analog VLSI, *Neural Comput.* **19**, 2581 (2007).
- [32] H. Nakao, Phase reduction approach to synchronisation of nonlinear oscillators, *Contemp. Phys.* **57**, 188 (2015).
- [33] J. T. C. Schwabedal, A. B. Neiman, and A. L. Shilnikov, Robust design of polyrhythmic circuits, *Phys. Rev. E* **90**, 022715 (2014).
- [34] J. A. White, C. C. Chow, J. Ritt, C. Soto-Trevino, and N. Kopell, Synchronization and oscillatory dynamics in heterogeneous, mutually inhibited neurons, *J. Comput. Neurosci.* **5**, 5 (1998).
- [35] T. J. Lewis and J. Rinzel, Dynamics of spiking neurons connected by both inhibitory and electrical coupling, *J. Comput. Neurosci.* **14**, 283 (2003).
- [36] N. Kopell and B. Ermentrout, Chemical and electrical synapses perform complementary roles in the synchronization of interneuronal networks, *Proc. Natl. Acad. Sci. U. S. A.* **101**, 15482 (2004).
- [37] G. Deco and V. K. Jirsa, Ongoing cortical activity at rest: criticality, multistability, and ghost attractors, *J. Neurosci.* **32**, 3366 (2012).
- [38] I. Belykh, V. Belykh, R. Jeter, and M. Hasler, Multistable randomly switching oscillators: The odds of meeting a ghost, *Eur. Phys. J.: Spec. Top.* **222**, 2497 (2013).
- [39] M. S. Al-Ghamdi, M. E. Khater, and E. M. Abdel-Rahman, Switching intermittency, *Appl. Phys. Lett.* **113**, 153501 (2018).
- [40] K. Pusuluri, S. Basodi, and A. Shilnikov, Computational exposition of multistable rhythms in 4-cell circuits, *Commun. Nonlinear Sci. Numer. Simul.* **83**, 105139 (2020).
- [41] E. Ott, C. Grebogi, and J. A. Yorke, Controlling Chaos, *Phys. Rev. Lett.* **64**, 1196 (1990).
- [42] A. Balanov, N. Janson, D. Postnov, and O. Sosnovtseva, *Synchronization: From Simple to Complex* (Springer, New York, 2009).
- [43] M. Bartos, I. Vida, and P. Jonas, Synaptic mechanisms of synchronized gamma oscillations in inhibitory interneuron networks, *Nat. Rev. Neurosci.* **8**, 45 (2007).
- [44] J. C. Smith, A. P. L. Abdala, H. Koizumi, I. A. Rybak, and J. F. R. Paton, Spatial and functional architecture of the mammalian brain stem respiratory network, *J. Neurophysiol.* **98**, 3370 (2007).
- [45] C. M. Michel and D. Brunet, EEG source imaging: a practical review of the analysis steps, *Front. Neurol.* **10**, 325 (2019).

- [46] R. D. Traub, M. A. Wittington, I. M. Stamford, and J. G. Jefferys, A mechanism for generation of long-range synchronous oscillations in the cortex, *Nature (London)* **383**, 621 (1996).
- [47] M. von Krosigk, T. Bal, and D. A. McCormick, Cellular mechanism of a synchronized oscillation in the thalamus, *Science* **261**, 361 (1993).
- [48] C. C. Canavier and R. A. Tikidji-Hamburyan, Globally attracting synchrony in a network of oscillators with all-to-all inhibitory pulse coupling, *Phys. Rev. E* **95**, 032215 (2017).
- [49] Z. G. Esfahani, L. L. Gollo, and A. Valizadeh, Stimulus-dependent synchronization in delayed-coupled neuronal networks, *Sci. Rep.* **6**, 23471 (2016).
- [50] M. Larkum, M. G. Rioult, and H.-R. Lüscher, Propagation of action potentials in the dendrites of neurons from rat spinal cord slice cultures, *J. Neurosci.* **21**, 9478 (2001).
- [51] X.-J. Wang and J. Rinzel, Alternating and synchronous rhythms in reciprocally inhibitory model neurons, *Neural Comput.* **4**, 84 (1992).
- [52] D. S. Goldobin and A. Pikovsky, Antireliability of noise-driven neurons, *Phys. Rev. E* **73**, 061906 (2006).
- [53] P. Channell, I. Fuwape, A. B. Neiman, and A. L. Shilnikov, Variability of bursting patterns in a neuron model in the presence of noise, *J. Comput. Neurosci.* **27**, 527 (2009).
- [54] M. I. Rabinovich, R. Huerta, and P. Varona, Heterosclinic Synchronization: Ultrasubharmonic Locking, *Phys. Rev. Lett.* **96**, 014101 (2006).
- [55] J. J. Torres, I. Elices, and J. Marro, Efficient transmission of subthreshold signals in complex networks of spiking neurons, *PLoS One* **10**, e0121156 (2015).
- [56] A. Samardak, A. Nogaret, N. B. Janson, A. G. Balanov, I. Farrer, and D. A. Ritchie, Noise-Controlled Signal Transmission in a Multithread Semiconductor Neuron, *Phys. Rev. Lett.* **102**, 226802 (2009).
- [57] R. Latorre, J. J. Torres, and P. Varona, Interplay between subthreshold oscillations and depressing synapses in single neurons, *PLoS One* **11**, e0145830 (2016).
- [58] I. Kupfermann and K. R. Weiss, The command neuron concept, *Behav. Brain Sci.* **1**, 3 (1978).
- [59] E. Marder and V. Thirumalai, Cellular, synaptic and network effects of neuromodulation, *Neural Networks* **15**, 479 (2002).
- [60] K. Nakada, T. Asai, and Y. Amemiya, An analog CMOS central pattern generator for interlimb coordination in quadruped locomotion, *IEEE Trans. Neural Networks* **14**, 1356 (2003).
- [61] T. Pfeil, J. Jordan, T. Tetzlaff, A. Grübl, J. Schemmel, M. Diesmann, and K. Meier, Effect of Heterogeneity on Decorrelation Mechanisms in Spiking Neural Networks: A Neuromorphic-Hardware Study, *Phys. Rev. X* **6**, 021023 (2016).
- [62] M. Lodi, A. Shilnikov, and M. Storace, Design of synthetic central pattern generators producing desired quadruped gaits, *IEEE Trans. Circuits Syst.: I* **65**, 1028 (2018).
- [63] A. Nogaret, E. L. O'Callaghan, R. M. Lataro, H. C. Salgado, C. D. Meliza, E. Duncan, H. D. I. Abarbanel, and J. F. R. Paton, Silicon central pattern generators for cardiac diseases, *J. Physiol.* **593**, 763 (2015).
- [64] F. Broccard, S. Joshi, J. Wang, and G. Cauwenberghs, Neuromorphic neural interfaces: from neurophysiological inspiration to biohybrid coupling with nervous systems, *J. Neural Eng.* **14**, 041002 (2017).